Optica Applicata, Vol. XIX, No. 1, 1989

Holographic moire contouring. Sensitivity and application constraints*

E. SIMOVA, V. SAINOV

Central Laboratory of Optical Storage and Processing of Information, Bulgarian Academy of Sciences, Sofia 1113, P.O. Box 95, Bulgaria.

The sensitivity and application constraints of holographic moire contouring of diffusely-reflecting objects are investigated. The basic theoretical relationships for determining the distance between the contouring planes are derived. The limitations imposed by the relief of the investigated object, contrast of interference fringes, and parameters of the optical configuration, forming the image, are discussed. A fair agreement between the theoretical and experimental results is observed.

1. Introduction

Holographic moire contouring is based on modulating an interference pattern by the object relief [1], [2]. The object is illuminated from two directions, symmetrical with respect to the surface normal, by collimated laser light and a double-exposure image-plane hologram is recorded at two different angles. A high-frequency carrier interference pattern is superposed on the reconstructed image, modulated by low-frequency fringes of equal relief. In order to eliminate the carrier frequency and to extract the contour map of the object, coherent optical filtering in the frequency plane is employed. This method is confirmed experimentally in [3], [4]. The aim of the present work is to determine the sensitivity and application constraints of holographic moire contouring by investigating the boundary conditions linked with the object, optical system, recording and processing.

2. Theory

2.1. Basic equations in holographic moire contouring

The optical path change δ, $\Delta\Phi = \frac{2\pi}{\lambda}\delta$, brought about by changing the illumination angle is derived by SCIAMMARELLA [2]. The intensity distribution in the interference pattern, reconstructed from the hologram for one-beam illumination of the object is

* This work was supported by the Committee of Science under contract No. 382.

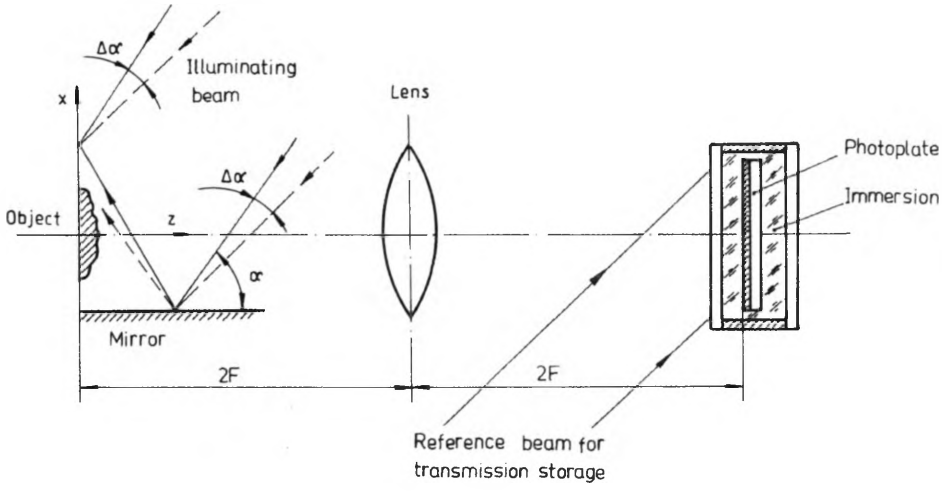

Fig. 1. Recording arrangement for holographic moire contouring

$$I_1 = I_0(1+\cos \Delta \Phi_1) = I_0\left\{1+\cos\left[\frac{2\pi}{\lambda}(x\cos\alpha_1 \sin \Delta\alpha_1 - z\sin\alpha_1 \sin\Delta\alpha_1)\right]\right\} \tag{1}$$

where α is the illumination angle, $\Delta\alpha$ is the illumination angle change ($\Delta\alpha \ll \alpha$), and I_0 is the background intensity. When a second illuminating beam is introduced (Fig. 1), symmetrical to the first one with respect to the normal to the object surface

$$\alpha_2 = -\alpha_1; \quad \Delta\alpha_2 = -\Delta\alpha_1; \quad |\alpha_2| = |\alpha_1| = \alpha; \quad |\Delta\alpha_2| = |\Delta\alpha_1| = \Delta\alpha.$$

The corresponding intensity distribution is

$$I_2 = I_0(1+\cos\Delta\Phi_2) = I_0\left\{1+\cos\left[\frac{2\pi}{\lambda}(x\cos\alpha\sin\Delta\alpha + z\sin\alpha\sin\Delta\alpha)\right]\right\}. \tag{2}$$

On reconstruction, the interference patterns superpose and an additive moire is observed which produces fringes of equal relief. The resulting intensity is

$$I = I_1 + I_2 = 2I_0\left[1+\cos\left(\frac{\Delta\Phi_1+\Delta\Phi_2}{2}\right)\cos\left(\frac{\Delta\Phi_1-\Delta\Phi_2}{2}\right)\right]$$

$$= 2I_0\left[1+\cos\left(\frac{2\pi}{\lambda}x\cos\alpha\sin\Delta\alpha\right)\cos\left(\frac{2\pi}{\lambda}z\sin\alpha\sin\Delta\alpha\right)\right]. \tag{3}$$

The two illuminating beams must overlap over the entire investigated surface. High contrast of the carrier interference pattern is achieved if the intensities of the two reflected waves in the recording plane are equal. This condition is fulfilled by diffusely-reflecting objects with small slopes. The equation of moire fringes which are observed as areas of minimal contrast in the carrier interference pattern is

$$\frac{2\pi}{\lambda}z(x)\sin\alpha\sin\Delta\alpha = (2N+1)\frac{\pi}{2}; \quad N = 0, 1, 2, \ldots . \tag{4}$$

Equation (4) describes a family of secant planes, perpendicular to the z-axis with a pitch

$$\Delta z = \frac{\lambda}{2 \sin \alpha \sin \Delta \alpha}. \tag{5}$$

The equation of the bright fringes of the carrier interference pattern is

$$\frac{2\pi}{\lambda} x \cos \alpha \sin \Delta \alpha = 2\pi N, \qquad N = 0, 1, 2, \ldots . \tag{6}$$

The pitch Δx along the x-axis and the carrier frequency f_x are, respectively,

$$\Delta x = \frac{\lambda}{\cos \alpha \sin \Delta \alpha}, \tag{7}$$

$$f_x = (\Delta x)^{-1} = \cos \alpha \sin \Delta \alpha / \lambda. \tag{8}$$

2.2. Constraints on the investigated object slope

To eliminate the carrier grating along the x-axis and to enhance the contrast of the contour fringes, the image, reconstructed from the hologram, is photographed. The transparency obtained is subjected to coherent optical filtering, as shown in Fig. 2. Only the plus-one or minus-one orders are transmitted and after the inverse Fourier transform the contour map of the investigated object is recorded. Diffraction orders should not overlap in the frequency plane. In the ideal case we consider only the spatial frequencies related to the change in slope of the investigated object. That is why a local spatial frequency is introduced [5], which is defined as

$$f_L = \frac{1}{\pi} \frac{\partial [\Delta \Phi(x)]}{\partial x}, \qquad \Delta \Phi = \frac{2\pi}{\lambda} z(x) \sin \alpha \sin \Delta \alpha, \tag{9}$$

$$f_L = \frac{2 \sin \alpha \sin \Delta \alpha}{\lambda} \frac{\partial z(x)}{\partial x}. \tag{10}$$

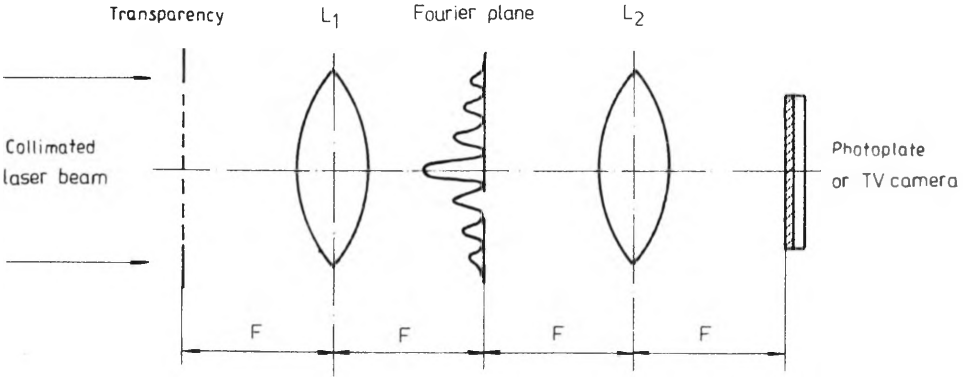

Fig. 2. Arrangement for coherent optical filtering in holographic moire contouring

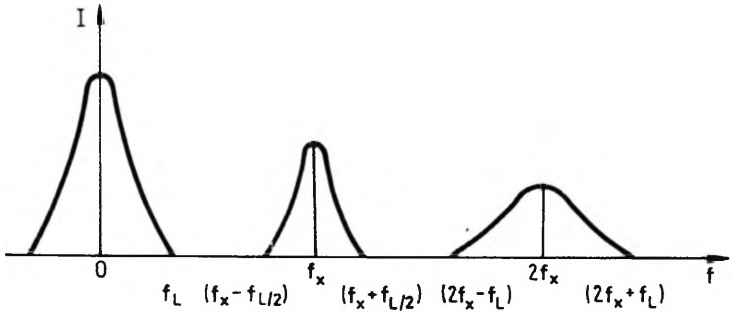

Fig. 3. Intensity distribution over spatial frequencies in the Fourier plane

Normally, photographic recording is non-linear and this contributes to contrast enhancement of the interference fringes. We shall consider the possibilities for separating the diffraction orders. When the dependence of the transparency transmission on the recorded intensity is quadratic, one may write

$$t \sim (I_1 + I_2)^2 = (2I_0)^2 \left[1 + \cos\left(\frac{\Delta\Phi_1 + \Delta\Phi_2}{2} \right) \cos\left(\frac{\Delta\Phi_1 - \Delta\Phi_2}{2} \right) \right]^2$$

$$= I_0^2 \left\{ 5 + 2\cos(\Delta\Phi_1)\cos(\Delta\Phi_2) + 8\cos\left(\frac{\Delta\Phi_1 + \Delta\Phi_2}{2} \right) \cos\left(\frac{\Delta\Phi_1 - \Delta\Phi_2}{2} \right) \right.$$

$$\left. + \cos(\Delta\Phi_1 + \Delta\Phi_2)\cos(\Delta\Phi_1 - \Delta\Phi_2) \right\}. \tag{11}$$

The above equation shows that non-linear recording results in the appearance of additional terms. In the frequency plane the second-order term is twice as wide as the first-order term. The intensity distribution in the spectrum (only one half-plane is examined) is schematically shown in Fig. 3. The condition for separation of the diffraction orders in the Fourier plane is of the form

$$(f_x - 1/2 f_L)_{\min} \geqslant f_{L\max},$$
$$2(f_x - 1/2 f_L)_{\min} \geqslant (f_x + 1/2 f_L)_{\max}. \tag{12}$$

Substituting f_x and f_L for expression (8) and (10), the condition takes the form

$$\frac{\partial z(x)}{\partial x} \leqslant 1/3 \operatorname{cotan} \alpha. \tag{13}$$

This is a strong constraint on the maximum allowable slope of the investigated object. It also satisfies the requirements for non-shading the investigated surface in the double-beam illumination.

2.3. Contrast of the carrier interference fringes in some simple cases of diffusely-reflecting objects

The contrast of the carrier interference fringes as a function of the shift of homologous rays in the image plane is investigated by SCIAMMARELLA and SCIAMMARELLA et al. [2], [6]. This problem is extremely important for holographic moire, since the contrast of the moire fringes depends on the contrast of the carrier fringes. The former is lower and does not exceed 1/2 for sinusoidal modulation [7]. CELAYA and TENTORI investigate in detail the interference pattern contrast in different kinds of displacements of a diffusely-reflecting object [8]. This analysis will be employed in the present considerations.

The contrast of the interference fringes is determined by the degree of correlation between the two speckle structures in the image plane, and Eqs. (1) and (2) take the form

$$I = I_0\{1+\gamma\cos[\Delta\Phi(x_i, y_i)]\}. \tag{14}$$

On recording with unit magnification through a circular aperture, the contrast of the fringes γ is given by the expression

$$\gamma = \frac{\iint \frac{2J_1(\pi a)}{\pi a}\frac{2J_1(\pi a')}{\pi a'}dx_0\,dy_0}{\iint\left|\frac{2J_1(\pi a)}{\pi a}\right|^2 dx_0\,dy_0} \tag{15}$$

where

$$a = \frac{\varrho}{2F}[(x_0-x_i)^2+(y_0-y_i)^2]^{1/2},$$

$$a' = \frac{\varrho}{2F}\left\{\left[(x_0+T_x)\left(1-\frac{T_z}{2F}\right)-x_i\right]^2+\left[(y_0+T_y)\left(1-\frac{T_z}{2F}\right)-y_i\right]^2\right\}^{1/2},$$

ϱ and F are the radius and focal length, respectively, of the lens, forming the image, and T_x, T_y and T_z are the displacement components of each point on the object surface.

The change in illumination angle is i dentical to a fictitious tilt of the object, as shown in Fig. 4. The displacement components of each point of the object for a tilt in the (x, z)-plane are

$$T_x = x_0(\cos\beta-1), \qquad T_y = 0, \qquad T_z = x_0\sin\beta. \tag{16}$$

The change in the optical path δ along the direction of observation (z-axis), caused by the change in the illumination angle, is equal to that caused by tilting the object,

$$\delta = |\vec{T}|. \tag{17}$$

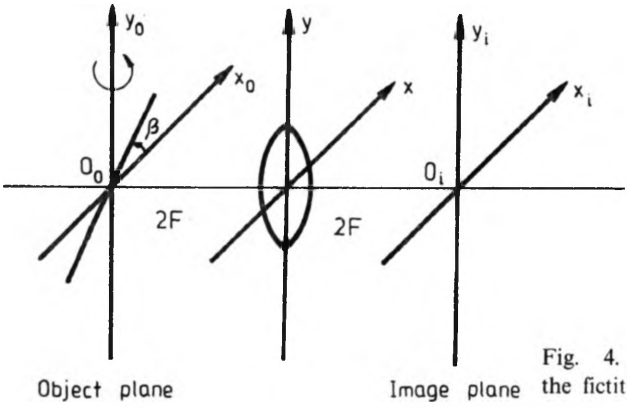

Fig. 4. Geometrical scheme for analysis of the fictitious tilt

Therefore, at small displacement angles

$$T_x \approx 0, \quad T_z = x_0 \cos\alpha \sin \Delta\alpha. \tag{18}$$

The shift between the images of identical points is expressed as a distance between the maxima of the Bessel functions for non-displaced and displaced points. In the first case the Bessel function maximum lies in the point with coordinates (x_i, y_i) in the image plane. In the case of displacement the coordinates of the maximum are $[x_i(1 + x_i/2F \cos\alpha \sin \Delta\alpha), y_i]$. The shift between the two maxima $|D_x|$ in x-direction, which is also the distance between the homologous rays in the image plane (Fig. 5), is given by the expression

$$|D_x| = \left|\frac{x_i^2}{2F} \sin \Delta\alpha \cos\alpha\right|. \tag{19}$$

The radius of the Bessel function is found from the first zero at a value of the argument 3.83. The first zero of the Bessel function for the case of displacement is located on an ellipse with the above center. When the object is tilted in the (x, z)-plane, the interference fringes are straight lines, located on the object surface, parallel to the y-axis. That is why we consider the shift between the homologous rays

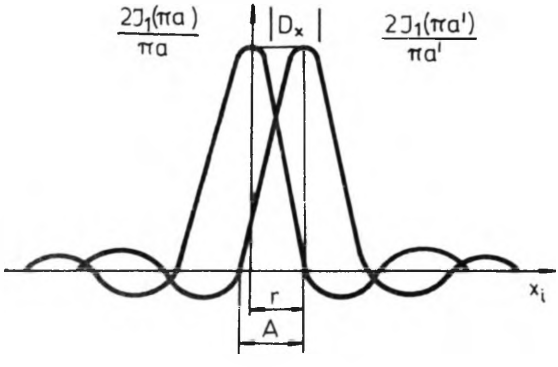

Fig. 5. Shift of the maxima of Bessel functions on decorrelation of the wavefronts in the image plane

and the loss of correlation in x-direction. The contrast of the fringes diminishes with increasing $|D_x|$ and becomes zero when $|D_x|$ is equal to the radius r of the Bessel function in the no-displacement case, or to the major half-axis of the ellipse A of the displaced Bessel function (Fig. 5)

$$|D_x| = r = 1.22\lambda F/\varrho. \tag{20}$$

From Equations (19) and (20) one can find the boundary angle of rotation of the illuminating beam at which the correlation between the wavefronts vanishes

$$\Delta\alpha_{\max} = \arcsin\left[\frac{2.44\,\lambda F^2}{\varrho\, x_i^2 \cos\alpha}\right]. \tag{21}$$

The analysis for the three-dimensional case is made for a cone with a base angle θ. The axis of the cone coincides with the z-axis and its vertex is taken to be in the origin of the coordinate system. We confine our considerations for a tilt in the (x, z)-plane. The components of the fictitious displacement of each point on the object, expressed in terms of the illumination angle change $\Delta\alpha$, are

$$\begin{aligned} T_z &\approx x_0 \tan\theta \sin\Delta\alpha \cos\alpha \frac{(1-\tan\theta\tan\alpha)}{(1+\tan^2\theta)^{1/2}}, \qquad T_y = 0, \\ T_z &\approx x_0 \sin\Delta\alpha \cos\alpha \frac{(1-\tan\theta\tan\alpha)}{(1+\tan^2\theta)^{1/2}}. \end{aligned} \tag{22}$$

By analogy with the two-dimensional analysis we determine the shift between the maxima of the Bessel functions along the x-axis. Disregarding the second-order terms, we get

$$|D_x| = \left| x_i \sin\Delta\alpha \cos\alpha \frac{(1-\tan\theta\tan\alpha)}{(1+\tan^2\theta)^{1/2}} \left(\tan\theta - \frac{x_i}{2F}\right)\right|. \tag{23}$$

The maximum rotation angle at which the correlation of the wavefronts is not yet lost (fringe contrast tends to zero), is given by the expression.

$$\sin\Delta\alpha_{\max} = \left| \frac{(1=\tan^2\theta)^{1/2}}{(1-\tan\theta\tan\alpha)\cos\alpha} \frac{\left[\left(1-\dfrac{1.22\lambda F}{x_i}\right)-1\right]}{\left(\tan\theta-\dfrac{x_i}{2F}\right)}\right|. \tag{24}$$

From Equation (24) it is obvious that the method is inapplicable for $\tan\theta\tan\alpha = 1$.

The model described takes into account the decline in contrast of interference fringes, due to the less of wavefront correlation in the ideal case. It does not take into account the influence of the optical system aberrations, image defocusing, signal-to-noise ratio of the recording material, the ratio between the intensities of the interfering waves.

2.4. Constraints on the depth of the investigated object

If contour fringes with high contrast are to be observed, the longitudinal displacement of the image between exposures must not exceed the depth of field of the objective. The constraint on the maximal depth of the investigated object is derived from the condition $T_z \leqslant \lambda (F/\varrho)^2$ [9]. In the case of a three-dimensional object (a cone), the boundary condition for the maximal depth is derived from the relationships in Sections 2.2 and 2.3

$$z(x) \leqslant (F/\varrho)^2 (1 + 1/9 \operatorname{cotan} \alpha)^{1/2} \Delta z. \tag{25}$$

The above expression includes also the frequency constraint on the slope of the investigated object (13). This relationship links the depth of the object with the pitch of the contouring fringes, maximal slope and F-number of the optical system.

3. Experiments

3.1. Experimental set-up

The experimental set-up is shown in Fig. 1. A He-Ne laser with a wavelength 632.8 nm and output power 30 mW is employed. This set-up provides double symmetrical illumination with collimated laser light, image-plane hologram recording with magnification 1:1, and F-number $(F/2\varrho) = 2$. The optical system has a resolution of about 20 mm^{-1} in the recording plane for diffusely-reflecting objects, illuminated with laser light. The illumination angle can be varied with an accuracy of $\pm 0.5'$. A tank with an immersion liquid is used for improvement holographic characteristics of the recording and for real-time investigations.

3.2. Characteristics of the holographic recording

A major requirement for the light-sensitive materials in holographic interferometry investigations, and especially holographic moire, is a high signal-to-noise ratio. This requirement is met by the superfine-grain silver halide light-sensitive plates HP–650 with a gelatin-polyacrylamide carrying matrix. Additional hardening of the emulsion layer, necessary for interferometric investigations, is achieved through the use of an immersion liquid. The ratio between the intensities of the object and reference beams is $I_0/I_R \approx 1{:}5$. Development is accomplished with a modified composition of the holographic developer GP–3 without subsequent fixing. For an experimentally determined signal-to-noise ratio in excess of 100:1, the resolution in the reconstructed image of a diffusely-reflecting test-object is 15 lines mm. Maximal contrast of the interference fringes is achieved when the diffraction efficiencies in the double-exposure recording are equal. In our case the ratio between the two exposures is $E_1/E_2 = 0.8 \pm 0.2$, and $E_1 + E_2 = 1.5$ mJ/cm^2 [10].

3.3. Experimental results

To remove the carrier fringes along the x-axis and to extract the contour map of the object, the image, reconstructed from the hologram, is photographed and subjected to coherent optical filtering, as shown in Fig. 2. The transparency is recorded onto silver halide plates Agfa–Gaevert 10E 75 Holotest and developed in D–19. The lenses L_1 and L_2 for direct and inverse Fourier transform have focal lengths $F = 1000$ mm. Filtering of the diffraction order is accomplished in the back focal plane of L_1 by means of an adjustable slit and after the inverse Fourier transform the image is recorded.

The results from holographic moire contouring of a three-dimensional diffusely-reflecting object (a cone) are illustrated in Fig. 6–8 before and after optical

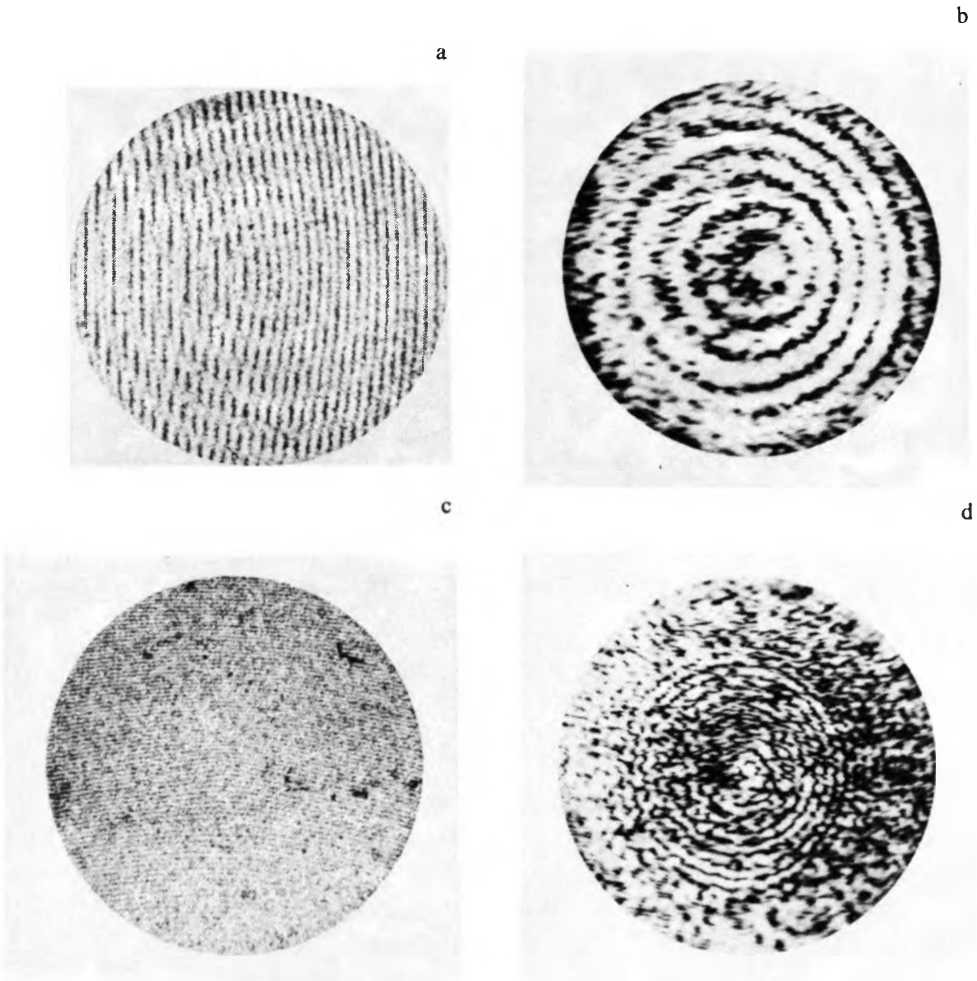

Fig. 6. Holographic moire contouring of a cone ($d = 10$ mm, $\theta = 15°$, $\alpha = 35°$): **a** – $\Delta\alpha = 8'$, $\Delta z = 237$ μm, before optical filtering; **b** – $\Delta\alpha = 8'$, $\Delta z = 237$ μm, after optical filtering; **c** – $\Delta\alpha = 22'$, $\Delta z = 86$ μm, before optical filtering; **d** – $\Delta\alpha = 22'$, $\Delta z = 86$ μm, after optical filtering

a b

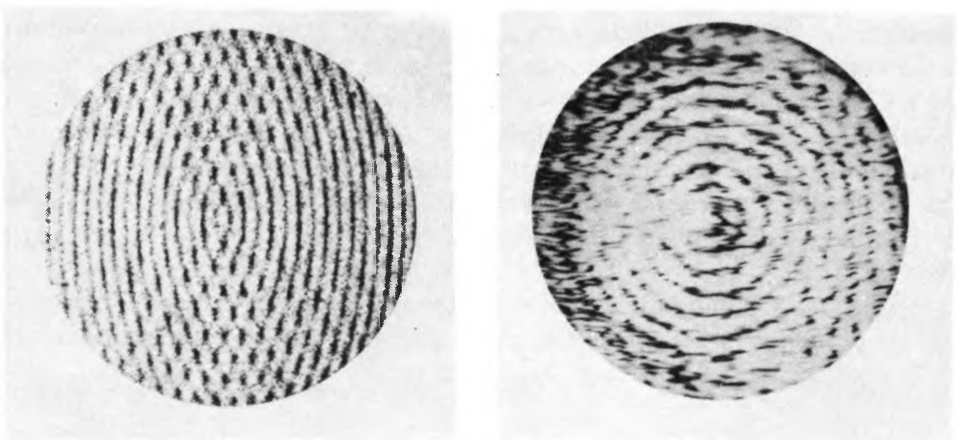

Fig. 7. Holographic moire contouring of a cone ($d = 10$ mm, $\theta = 30°$, $\alpha = 35°$): **a** – $\Delta\alpha = 6'$, $\Delta z = 316$ μm, before optical filtering; **b** – $\Delta\alpha = 6'$, $\Delta z = 316$ μm, after optical filtering

a b

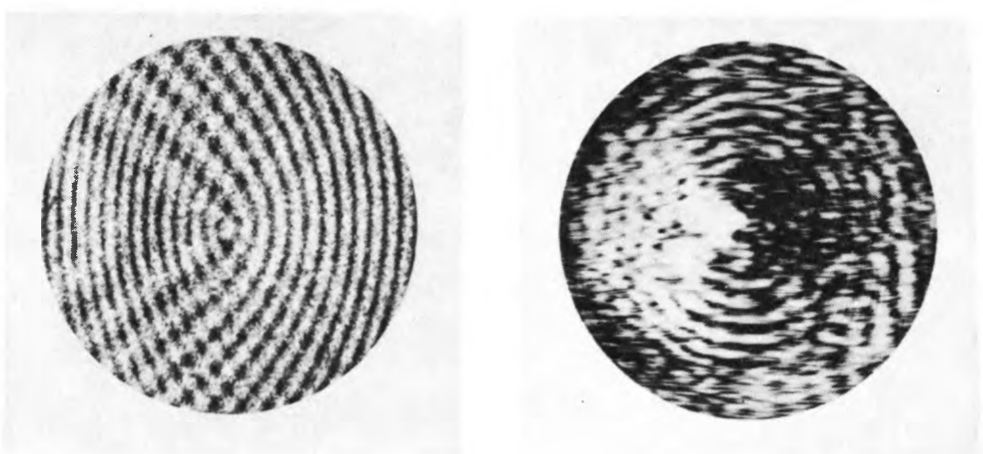

Fig. 8. Holographic moire contouring of a cone ($d = 10$ mm, $\theta = 45°$, $\alpha = 35°$): **a** – $\Delta\alpha = 4'$, $\Delta z = 474$ μm, before optical filtering; **b** – $\Delta\alpha = 4'$, $\Delta z = 474$ μm, after optical filtering

filtering. The experiments were conducted at an illumination angle $\alpha = 35°$. The cone has a diameter of the base $d = 10$ mm and base angle $\theta = 15, 30, 45°$. Fig. 6**c**, **d** illustrate the case of a strong decrease in the contrast of the carrier and moire fringes at great rotation angles of the illuminating beams, and Fig. 7 and 8 illustrate the boundary condition for the slope of the investigated object.

3.4. Analysis of the results

The experimental results prove the validity of the boundary condition (13) which originates from the requirement for separation of the diffraction orders in the

frequency plane. Condition (13) is not fulfilled for cones with base angles 30° and 45° (Figs. 7, 8). In these cases the diffraction orders overlap along the x-axis and information about the contours of the object in this direction is lost. Objects with "steeper" slopes can be contoured at smaller illumination angles α (Fig. 1), Eq. (5). However, the sensitivity of the method decreases and so does the maximum angle of rotation. To raise the sensitivity, $\Delta\alpha$ must increase, but this results in deterioration of the contrast of interference fringes. At normal illumination the method is inapplicable, see Eq. (1). It is suitable for contouring objects with small slopes, which allows increasing the sensitivity without the risk of shading and improper filtering. For the recording geometry chosen ($\alpha = 45°$, $\alpha = 35°$, F-number $F/2\varrho = 2$) the maximum sensitivity of contouring is about 100 μm. The sensitivity of the method can also be increased by choosing an objective with a smaller F-number $F/2\varrho$, i.e., by increasing $\Delta\alpha_{\max}$ – the maximum rotation angle (24), but one should be aware of the larger speckle size. On one hand, the large size of the speckles allows greater displacements of the object, but, on the other hand, it restricts the maximum observable density of the fringes. The choice of the optical system for recording and optical processing is dictated by the requirements of the specific task. It should be noted that because of the small size of the transparency and the great focal length F of the Fourier lenses the mean size of the speckles $\sigma = 1.22\lambda(F/\varrho)$ in our case is great and commensurate to the distance between the contouring fringes. The great focal length is necessary for a better separation of the orders in the frequency plane. Usually, a compromise is sought.

3.5. Determination of the contrast of the carrier interference pattern

Experimental verification of the relationships between the contrast of the fringes and the wavefront decorrelation is accomplished for the case of a plane object and a cone with diffusely-reflecting surfaces. The density of the photographed interferograms is measured and the contrast of the fringes γ is calculated from the formula

$$\gamma = \frac{I_{\max} - I_{\min}}{I_{\max} + I_{\min}}.$$

In the literature the theoretical curves for the contrast of the interference fringes are plotted as functions of the displacement between the homologous rays in the image plane, normalized to the mean speckle size [2], [6]. The relationships derived in Section 2.3, make possible the determination of the displacement between the maxima of Bessel functions $|D_x| = f(\Delta\alpha)$. The theoretical and experimental results are compared in Fig. 9 (for the case of a plane object), and in Fig. 10 (for a three-dimensional diffusely-reflecting object, a cone with base angles $\theta = 15$, 30° and $\alpha = 45°$). The experimental data confirm the decrease in contrast with the increase in angle θ. The experimental curves exhibit a slower decrease in contrast for the boundary angles $\Delta\alpha$ than the theoretical curves, since the theoretical model does not take into account all factors influencing the contrast of the fringes (Sect. 2.3).

The precise quantitative estimation of the contrast of moire fringes is difficult to

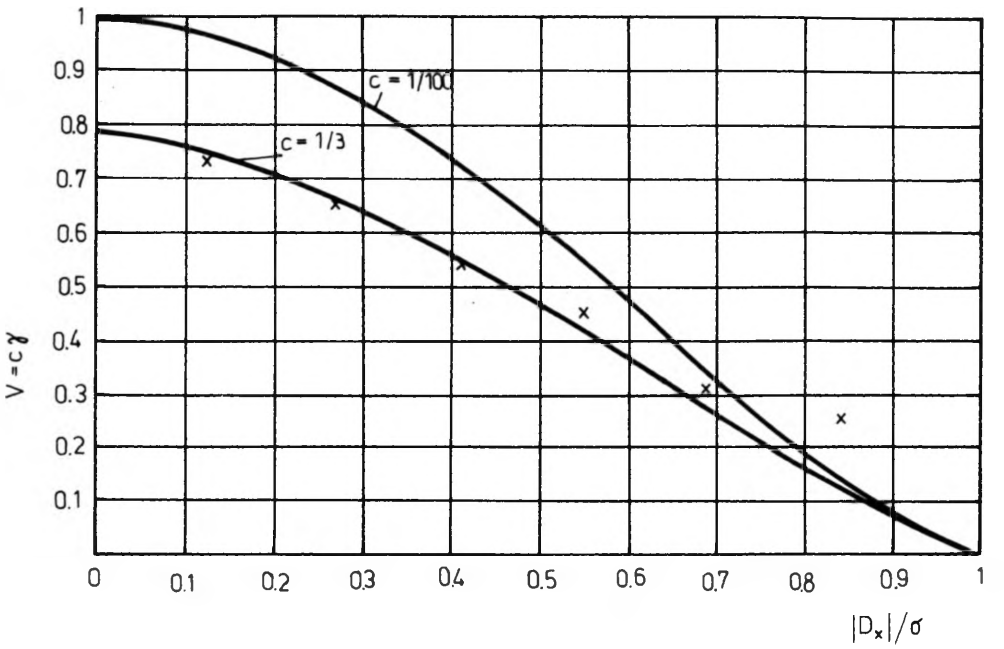

Fig. 9. Contrast of interference fringes as a function of the displacement of homologous rays, normalized to the speckle size, for a circular aperture and a plane diffusely-reflecting object; theoretical curves and experimental points (×)

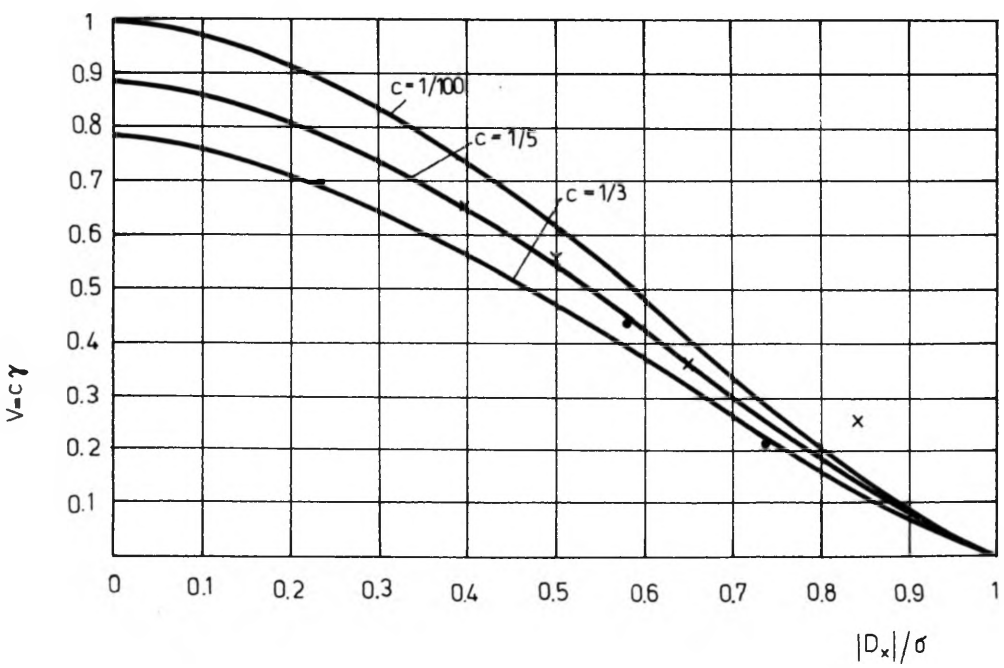

Fig. 10. Contrast of interference fringes as a function of the displacement of homologous rays, normalized to the speckle size, for a circular aperture and a three-dimensional diffusely-reflecting object: theoretical curves and experimental points at $\theta = 15°$ (×), at $\theta = 30°$ (●)

make. It depends on the contrast of the carrier fringes. When the displacement $|D_x|$ approaches the size of the speckles σ, the contrast diminishes sharply, which sets an upper limit to the measurements by the holographic moire method. If a requirement is imposed that the resulting contrast of the moire fringes should be 0.25, it can be shown that in the case of a circular aperture $|D_x| \leqslant 0.6\ \sigma$.

The depth of the investigated object for image-plane holograms, reconstructed with coherent light, is limited also by the parameters of the optical observation system, which is not taken into account in the limiting condition (25) [11].

4. Summary

The present work deals with theoretical and experimental investigations into the possibilities of holographic moire contouring of diffusely-reflecting objects. The method is non-contacting and features simplicity of the optical configuration. It is suitable for contouring objects of small slope. The necessity for collimated illumination, like in the other holographic contouring methods, confines its application to small-sized objects. The problem of fringe localization is not essential. The method can be used in real-time investigations, in which the pitch of the contour fringes along the direction of observation (z-axis) can be varied by changing the illumination angle. The sensitivity and range of measurements are relatively limited. They depend on the geometry of the recording set-up and on the characteristics of the optical system, used for image formation.

Anknowledgements – The authors appreciate the assistance, offered to them by their colleagues in the Central Laboratory of Optical Storage and Processing of Information, who produced high-quality light-sensitive materials for the experiments.

References

[1] Beranek W. J., Bruinsma A. J., [In] *4th SESA Int. Congress on Experimental Mechanics*, Boston 1980, p. 47.
[2] Sciammarella C. A., Opt. Eng. **21** (1982), 447.
[3] Sciammarella C. A., Sainov V., Simova E., *Holographic moire contouring* (to be published).
[4] Sainov V., Simova E., Compt. Rend. Acad. Bulg. **41** (1988), 39.
[5] Takeda M., Mutoh K., Appl. Opt. **22** (1983), 3977.
[6] Sciammarella C. A., Rastogi P. K., Jaquot P., Narayanan R., J. Exp. Mech. **22** (1982), 52.
[7] Rastogi P. K., Jaquot P., Pflug L., Opt. Acta **30** (1983), 1067.
[8] Celaya M., Tentori D., Appl. Opt. **25** (1986), 2796.
[9] Erf R. K., *Holographic Nondestructive Testing*, Academic Press, New York, London 1974, p. 105.
[10] Sainov V., Simova E., [In] *Proc. Nat. Conf. Optica '87*, Bulgaria (in Bulgarian), p. 411.
[11] Klimenko I. S., *Image Plane Holography and Speckle Interferometry*, [Ed.] Nauka, Moscow 1985 (in Russian), p. 20.

Received October 11, 1988
in revised form December 8, 1988

Голографическое очертание типа муаре. Чувствительность и аппликационные ограничения

Исследована чувствительность голографического очертания типа муаре для предметов диффузионно отражающих, а также ограничения его применения. Введены основные теоретические соотношения для определения удаленности между плоскостями очертания. Продискутированы ограничения, вводимые рельефом исследуемого предмета, контраст интерференционных линий и параметры оптической конфигурации, формирующей образ. Получено достаточное согласие между теоретическими и экспериментальными результатами.